FRGS15-165-0406 - Final report

Mathematical Analysis to Estimate Optimal Shunt Impedance for Piezoelectric Transducer to Maximize Vibration Energy Dissipation in Non-Deterministic Sub-Systems

Asan G A Muthalif [*], Azni N Wahid
asan@iium.edu.my
Smart Structures, Systems & Control Research Laboratory (S^3 CRL)
Department of Mechatronics Engineering, International Islamic University Malaysia,
Jalan Gombak, 53100 Kuala Lumpur, Malaysia

Engineering systems such as aircrafts, ships and automotive are built-up structures fabricated from many components that can be classified as deterministic substructure (DS) and non-deterministic substructure (Non-DS). Non-DSs are subjected to high-frequency vibration which produced response that cannot be described mathematically using deterministic method. This makes vibration energy harvesting tricky due to the combined modal response which produce no visible distinct peaks. Piezoelectric (PZT) transducer connected to a shunt circuit is an attractive choice to harvest vibration energy from a Non-DS. Using Hybrid modelling equation, the impedance of the circuit to be attached to the Non-DS needs to be complex conjugate of the impedance faced by the Non-DS at its connection point. The shunt circuit of the PZT shunt harvester is designed such that the impedance is complex conjugate of its inherent capacitance parallel with impedance faced by the host structure at the connection area. In the first part of this research, the impedance faced by the Non-DS at the connection area is estimated using effective line mobility of an infinite thin plate under moment excitation by a square PZT patch using double integration of the infinite mobility which resulted to a hypergeometric function. The analytical model is compared with the average response of a randomized finite thin plate via Monte Carlo simulation which managed to significantly cut computational time to ~40 times shorter compared to using the finite method. Using findings from this part, the implementation of the designed shunt circuit using electronic components is carried out. One possible circuit configuration that closely resembles the theoretical impedance derived is realized by application of two negative impedance converters (NICs) utilizing op-amps, in order to replicate the negative capacitance, C and negative RL in series.

Keywords: High-frequency vibration energy harvesting, Piezoelectric shunt damper, optimal impedance, effective line moment mobility, the Hybrid modeling method

Deterministic substructures (DS) are structures that are subjected to long wavelength deformation considered as low-frequency vibration while non-deterministic substructures (Non-DS) are structures that are subjected to short wavelength deformation termed as high-frequency vibration. The term ‘high’ is not simply numerical; it implies that the frequency range extends to many times the fundamental natural frequency of a structure under consideration [1]. In Statistical Energy Analysis (SEA), modal overlap factor (MOF) is used to quantify the degree of overlap in modal response i.e. the ratio of the half-power bandwidth to the local average interval between natural frequencies [2, 3].

$$MOF(\omega) = n\omega\eta = \frac{A}{4\pi}\sqrt{\frac{\rho h}{D}}\omega\eta \quad (1)$$

where n is the modal density, η is the modal loss factor, ω frequency in rad/s, A is the surface area of the structure ρ, h and D are the density, thickness and the flexural rigidity of the structure, respectively. At low frequency range (MOF<1), individual modal responses are distinctly visible therefore response can be effectively simulated using the conventional finite element method (FEM). The mid frequency range (1<MOF<2) is when the modal response is beginning to overlap and MOF>2 is the high frequency range where: (i) the vibration response is increasingly sensitive to uncertainties [1, 4, 5] and (ii) no distinct resonant peaks are visible in the response since the modal responses are combined to be broader peaks (see Figure 1) [6]. Additionally, vibrations at higher frequency range has much smaller wavelength than the lower modes, which means i) higher number of degrees of freedom is needed to model the response that requires high computational time and cost, ii) the wave can efficiently propagate through smaller cracks in structures and later intensifies the damage.

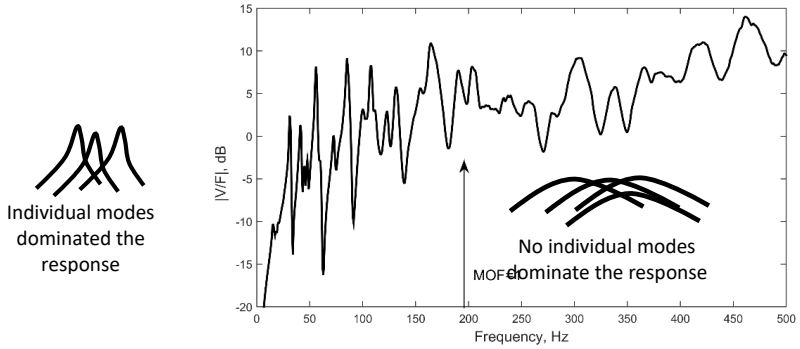

Figure 1: Frequency response function of a rectangular plate to show modal overlap factor, MOF

An attempt to develop active control for high frequency vibration (structural response with MOF>2) control has been discussed in work by Muthalif [6] where they used skyhook damper (equivalent to point force) to dissipate energy from a Non-DS. The optimal value for the skyhook damper constant is achieved by doing the first derivative of the hybrid Finite Element/SEA (FE/SEA) equation coined by Langley [7]. This paper will attempt to dissipate vibration energy from a thin plate vibrating at high-frequency range by using a piezoelectric (PZT) patch transducer as a passive damper by connecting a shunt circuit through its terminal, known as shunt damping [8, 9]. The crux of this research will be to find the optimal circuit impedance of the PZT shunt damper to maximize energy dissipation from the Non-DS.

In order to use a PZT shunt damper as medium of energy dissipation from a Non-DS, the effect of a PZT patch on a Non-DS needs to be investigated due to its different forcing distributions compared to a skyhook damper. The approach taken here is to model a PZT patch transducer as line moment exciter on a randomized thin plate and to estimate its mobility function using infinite mobility term. This finding will be crucial for determining the optimal electrical circuit of the shunt damper by utilizing hybrid (FE/SEA) modelling method which found out to be equivalent to impedance matching method [6, 10, 11].

2.0 DERIVATION OF OPTIMAL IMPEDANCE FOR NON-DS CONTROL

The hybrid Finite Element/SEA (FE/SEA) modelling approach treats a complex built-up system as a combination of components with fully deterministic properties (DS) and substructure that have high degree of randomness (Non-DS) [7, 10, 12]. Consider the simplest form of built-up structure where a shunted PZT patch is directly acting on a randomized thin plate; the patch with its circuit is treated as a DS and the host substructure as a Non-DS (
Figure 2). The strategy for Non-DS vibration suppression is investigated by finding the optimal impedance of the DS when the energy loss at the DS is maximized, using the first derivative of hybrid (FE/SEA) method [13]. The equation used to find the Non-DS energy (SEA part of the hybrid method) for the system in
Figure 2 is:

$$\left(\omega\eta_{d,1}n_1 + \omega\eta_1 n_1\right)\frac{E_1}{n_1} = P_{in} \tag{2}$$

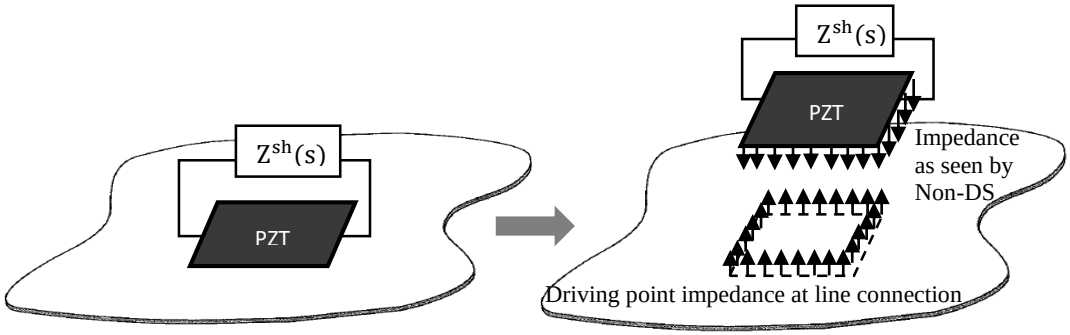

Figure 2: A PZT patch with shunt circuit, $Z^{sh}(s)$ acting on a Non-DS

where η_1 and n_1 are the loss factor and modal density of the Non-DS, $\eta_{d,1}$ is the loss factor of the DS (the controller), $\frac{E_1}{n_1}$ is the modal energy of the subsystem and P_{in} is the power input to the subsystem. If the power input to the Non-DS is fixed, then increasing the magnitude of $\omega\eta_{d,1}n_1$ will then decrease the energy of the Non-DS, $\frac{E_1}{n_1}(\omega\eta_1 n_1)$ which fulfils the control purpose. The first term in Eq. (2) is given by the hybrid method as:

$$\omega\eta_{d,k}n_k = \frac{2}{\pi}\sum_{rs} Im\left(\boldsymbol{D}_{d,rs}\right)\left(\boldsymbol{D}_{tot}^{-1} Im\{\boldsymbol{D}_{dir}^{k}\}\boldsymbol{D}_{tot}^{-H}\right)_{rs} \tag{3}$$

where $\boldsymbol{D}_{d,rs}$ is the complex dynamic stiffness matrix for the DS, $\boldsymbol{D}_{dir}^{k}$ is the complex direct dynamic stiffness matrix at the coupling points (line or area), $\boldsymbol{D}_{tot}$ is sum of $\boldsymbol{D}_{d,rs}$ and $\boldsymbol{D}_{dir}^{k}$, $\boldsymbol{D}_{tot}^{-H}$ is the inverse of hermitian transpose for $\boldsymbol{D}_{tot}$. The relationship between complex dynamic stiffness to structural impedance is $D_{d,DS} = j\omega Z_d$ $D_{d,DS} = j\omega Z_d$ and $D_{dir} = j\omega Z_\infty$ $D_{dir} = j\omega Z_\infty$ where Z_D $D_{dir} = j\omega Z_\infty$ Z_d is the impedance of the DS as "seen" by the Non-DS and $Z_\infty Z_\infty$ is the infinite plate driving point impedance at the connection between the DS and Non-DS. While this is unambiguous for a skyhook damper which is a mechanical damper with point junction, the impedance expression needs more fine definition for other types of controller; in this case, a PZT

shunt damper is an electromechanical transducer and has completely different forcing distribution and spatial connection with its host structure. Evidently, having the knowledge of mobility function of a structure can help to determine the design for an optimal controller for maximum energy dissipation from a Non-DS.

Consider *n* number of PZT shunt dampers on the Non-DS, the optimal impedance value for each of the DS in order to maximize the value of energy loss, $\eta_{d,1}$ is obtained by doing the first derivative of Eq. (3) with respect to both real part and imaginary part of $D_{d,k}$ for the k^{th} DS separately, which will lead to:

$$D_{dR,k} = -D_{dirR,k} \tag{4}$$

$$D_{dI,k} = D_{dirI,k} \tag{5}$$

Eqns. (4) and (5) are the optimal impedance for a DS, or specifically the optimal impedance of the k^{th} shunted PZT patch needed to minimize the Non-DS's energy which is essentially equivalent to the 'impedance matching technique'. In addition, the equations also illustrate that the optimal gain value for each deterministic controllers are independently-related to the direct dynamic stiffness of its non-deterministic host structure at their respective point/line/area connection. This finding will significantly simplify the controller's design. Further investigation using the above derivation also reveals that the energy ratio between a bare plate and a controlled plate using optimized DS becomes:

$$\frac{E_o}{E_c} = 1 + \left(\frac{N}{2\pi\omega\eta_o n}\right) \tag{6}$$

where *N* is the quantity of the optimized controller in this case it is the PZT patch with optimal shunt impedance. Evidently, as frequency is made higher, the energy ratio between a bare plate, $E_o E_o$ and a controlled plate, E_c will approach to unity, $\frac{E_o}{E_c} \approx 1 \frac{E_o}{E_c} \approx 1$; which implies that control for a Non-DS is ineffective at very high frequency. However, the number of controllers, *N* can be increased to alleviate this drawback as shown in Figure 3.

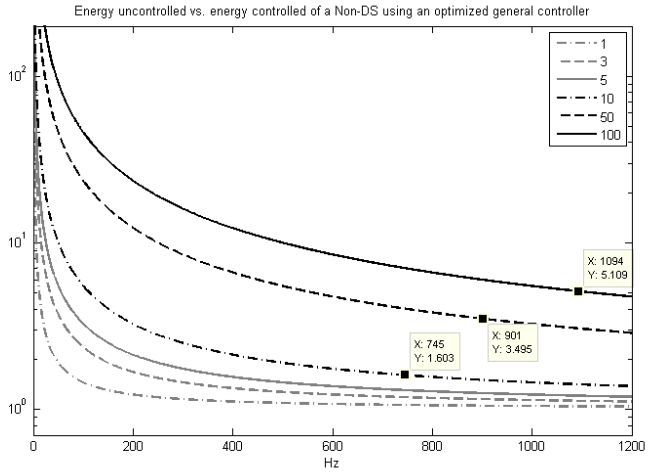

Figure 3: Energy uncontrolled vs. energy control of a Non-DS with different number of optimal general controller *N* as in Eq.(6)

3.0 DYNAMIC ELECTROMECHANICAL RESPONSE OF A PIEZOELECTRIC SHUNT DAMPER ON A RANDOMIZED THIN PLATE

To derive the equation of motion for a thin plate attached with a PZT patch shunt damper, the work in [14] is referred. Hagood and his co-worker showed how to use the constitutive equation for PZT material to obtain the general equation for a PZT in terms of the external current input and applied voltage. Rearranging the terms, the following is obtained:

$$\begin{bmatrix} I \\ \sigma_{pzt} \end{bmatrix} = \begin{bmatrix} Y^{EL} & sAe \\ -e^t t_p^{-1} & c^E \end{bmatrix} \begin{bmatrix} V \\ S \end{bmatrix} \tag{7}$$

$$Y^{EL} = Y^D_{PZT} + Y^{sh} \tag{8}$$

where I is the electric current, V is the electric voltage, A is the surface area perpendicular to the electrical field (diagonal matrix), t_p is the thickness of the patch, Y^{EL} is the electrical admittance and $Y^D_{PZT} = sC^s_{ps}$. The stress expression is updated as:

$$\sigma_{pzt} = [c^E + e^t \bar{Z}^{EL} (\varepsilon^S)^{-1} e]S - [e^t t_p^{-1} Z^{EL}]I \tag{9}$$

And the new modulus of elasticity for a shunted PZT patch is defined as:

$$c^{shunt} = [c^E + e^t \bar{Z}^{EL} (\varepsilon^S)^{-1} e] \tag{10}$$

where the matrix of non-dimensional electrical impedance is:

$$\bar{Z}^{EL} = Z^{EL}(Z^D_{PZT})^{-1} = (sC^s_{ps} + Y^{sh})^{-1} sC^s_{ps} \tag{11}$$

$\bar{Z}^{EL} = 1$ is for open circuit condition

The total equation of motion for a thin plate attached with a PZT patch connected to a shunt circuit, $Z^{sh}(s)$ becomes:

$$\begin{aligned} -\omega^2 \left(M_{plate} + M_{pzt} + M_{ptmass}\right) W_{mn,s} + \left(K_{plate} + K_{pzt} + \Gamma^T \bar{Z}^{EL} \varepsilon^{S^{-1}} \Gamma\right) W_{mn,s} \\ = \Gamma Z^{EL} I(\omega) + \phi_f F_i \end{aligned} \tag{12}$$

Solving for $W_{mn,s}$ yields

$$W_{mn,s} = \Delta_s{}^{-1} \Gamma Z^{EL} I(\omega) + \Delta_s{}^{-1} \phi_f F_i(\omega) \tag{13}$$

where $\Delta_s(\omega)$ is expressed as:

$$\Delta_s(\omega) = -\omega^2 \left(M_{plate} + M_{pzt} + M_{ptmass}\right) + \left(K_{plate} + K_{pzt} + \Gamma^T \bar{Z}^{EL} \varepsilon^{S^{-1}} \Gamma\right) \tag{14}$$

Since a simply-supported plate is used, the deflection of the plate during vibration can be assumed as the double series:

$$w(x,y,t) = \sum_m \sum_n W_{mn}(t)\,\phi_{mn} \tag{15}$$

$$\phi_{mn} = sin\frac{m\pi x}{L_x} sin\frac{n\pi y}{L_y} \tag{16}$$

The finite energy model of the plate-patch system can be written as:

$$E_{fin} = \frac{1}{2} W_{mn,s}^T K_{plate} W_{mn,s} \tag{17}$$

By neglecting the mass and stiffness of the PZT patch shunt damper, the mechanical dynamic stiffness matrix of deterministic part of the system in Figure 2 can be written as:

$$D_{d,PSD} = j\omega \Gamma^T \varphi_{M_{line}}^{-1} Z_{el} \quad \varphi_{\dot{\theta}_{line}}^{-1} \Gamma \tag{18}$$

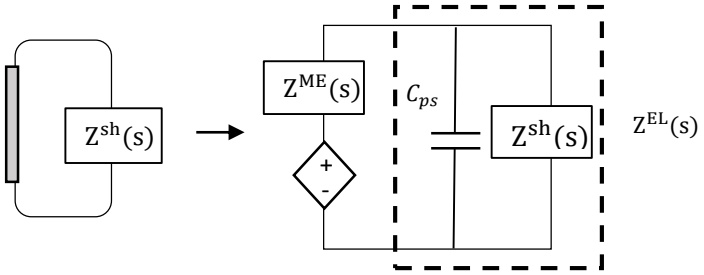

Figure 4: Physical model of a shunted PZT patch and its network analog

The term Γ is the electromechanical coupling matrix, $\varphi_{M_{line}}$ is the shape function for line moment along the edges of the patch for line connection, $\varphi_{\dot{\theta}_{line}}$ is the shape function for angular velocity along the edges of the patch for line connection, and Z_{el} is the electrical representation of the PZT shunt damper on the Non-DS, that is the electrical shunt impedance parallel with inherent capacitance impedance of the patch, $Z_{sh}||Z_{Cp}$ or:

$$Z_{el} = \frac{Z_{sh}}{1 + Z_{sh} C_p} \tag{19}$$

The main interest is to design the shunt circuit impedance, Z_{sh}, hence, solving for Z_{sh} in terms of direct dynamic stiffness, $\overline{D}_{dir} = \overline{D}_{Redir} + j\overline{D}_{Imdir}$ and letting $X_{Cp} = -\frac{1}{\omega C_p}$, the following is obtained:

$$Z_{sh} = \frac{\omega X_{Cp}{}^2 \overline{D}_{Imdir}}{\overline{D}_{Imdir}{}^2 + (-\overline{D}_{Redir} - \omega X_{Cp})^2} - j\frac{\overline{D}_{Imdir}{}^2 X_{Cp} + X_{Cp}\overline{D}_{Redir}(\overline{D}_{Redir} + \omega X_{Cp})}{\overline{D}_{Imdir}{}^2 + (-\overline{D}_{Redir} - \omega X_{Cp})^2} \tag{20}$$

The bar sign in $\bar{D}_{dir}$ signifies the equivalent electrical dynamic stiffness matrix, converted from its mechanical dynamic stiffness matrix, D_{dir} i.e.:

$$\bar{D}_{dir} = \varphi_{M_{line}} \Gamma^{-T} D_{dir} \Gamma^{-1} \varphi_{\dot{\theta}_{line}} \tag{21}$$

Using conditions in Eqns. (4) and (5) to obtain maximum energy dissipation at the deterministic controller and substituting in terms of infinite mechanical impedance will produce the following expressions:

$$Z_{sh} = \frac{{X_{Cp}}^2 \bar{Z}_{Re\infty}}{{\bar{Z}_{Re\infty}}^2 + (\bar{Z}_{Im\infty} + X_{Cp})^2} - j\frac{{\bar{Z}_{Re\infty}}^2 X_{Cp} + X_{Cp}\bar{Z}_{Im\infty}(\bar{Z}_{Im\infty} + X_{Cp})}{{\bar{Z}_{Re\infty}}^2 + (\bar{Z}_{Im\infty} + X_{Cp})^2} \tag{22}$$

Eq. (22) is therefore the optimal impedance for shunt circuit of the PZT shunt damper on a Non-DS in order to maximize energy dissipation which is the complex conjugate of its inherent capacitance, X_{Cp} parallel with mechanical-converted to-electrical impedance 'faced' by the Non-DS at the junction, $\bar{Z}_{\infty}$. The derivation of $\bar{Z}_{\infty}$ will be shown in the following subsection.

3.0 DERIVATION OF EFFECTIVE LINE MOMENT MOBILITY ON INFINITE THIN PLATE

3.1 Introduction

The concept of surface mobilities have been introduced and derived throughout the years to better approximate power transmission between contact region of source and receiver. In classical studies, the connection between the isolator and host structure is assumed to be point-like with assumption that the excitation area are less than approximately one-tenth of a wavelength [15, 16]. For obvious reason, this assumption is not accurate for PZT patch transducers in which the connection area generally has dimensions comparable to the governing wavelength. Hammer and Petersson in [17] introduced the concept of strip mobility to investigate power transmission to a thin plate excited by transverse strip excitation. Later, Norwood et al. [15] have developed the concept of surface mobility on circular contact area using time-averaged input power and effective mobility. The work was extended to square-shaped contact area by Li et al. [18] and Dai et al. [19] using a discretized model to find the effective point mobility and corresponding surface mobility.

3.2 Infinite mobilities model

In this paper, a multi-point connection model is employed through integration method in order to determine effective line mobility of an infinite thin plate excited by line moments induced by a PZT patch actuator termed as *effective line moment mobility*. The PZT patch is assumed to generate purely line moments at each of its edges. To acquire the effective *line moment* mobility, we must first derive the *effective point moment* mobility; that is the resulting angular velocity at one point on the plate by excitation moments from all connection points. Work by Ljunggeren in [20] had derived effective point mobility from expressions for point-excited fields where a source in the form of a force applied along infinite line can be regarded as infinite number of point forces. Reasonably, one can acquire effective point moment mobility generated by a *finite* line moment

on an infinite thin plate by following the same principle i.e. doing a definite integration of the angular displacement due to a *point* moment along the length of the line moment.

The angular displacement at position (r,α), in response to a couple of *point* moment M_u with orientation u which acts on a rigid indenter fixed to the plate is given by [16] as:

$$\theta_u{}'(r,\alpha) = \left(\frac{M_u}{j\omega}\right)\frac{\omega}{8D}\left\{sin(\alpha-\beta_p)\,sin(\alpha-\beta)\left[\left(H_0^{(2)}(k_Br) - j\frac{2}{\pi}K_0(k_Br)\right)\right.\right.$$
$$\left. - \frac{1}{k_Br}\left(H_1^{(2)}(k_Br) - j\frac{2}{\pi}K_1(k_Br)\right)\right]$$
$$\left. + \frac{cos(\alpha-\beta_p)\,cos(\alpha-\beta)}{k_Br}\left(H_1^{(2)}(k_Br) - j\frac{2}{\pi}K_1(k_Br)\right)\right\} \quad (23)$$

where $H_i^{(2)}(k_Br)$ is the second kind of Hankel function of the ith order, $K_i(k_Br)$ is the second kind of modified Bessel function of the ith order, $k_B = \sqrt[4]{\frac{\omega^2\rho h}{D}}$ is the bending wavenumber, r is distance between force applied and velocity measured, β is the angle between x-axis and moment arm, M_u and α is the angle between x-axis and the radius line that connects point (x_1, y_1) and (x_2, y_2). The angular displacement at a point resulting from *line* moment excitation with length b-a can be taken as:

$$\theta_u = \int_a^b \theta_u{}'(r)dr \quad (24)$$

where a and b are finite numbers which accounts for the length of the line moment and r is the distance between the response point and the moment excitation along the line.

$$r = \sqrt{(x_2-x_1)^2 + (y_2-y_1)^2} \quad (25)$$

Since angular velocity is taken at one fixed point (x_2, y_2), then the coordinate of the point moment will be the variable to be integrated.

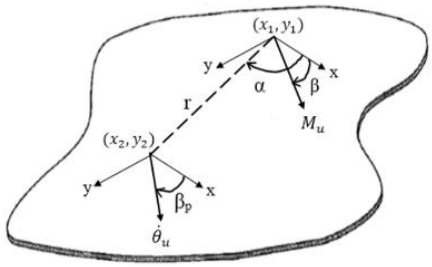

Figure 5: Sign conventions for resulting angular velocity at point (x_2, y_2) subjected by a point moment excitation at (x_1, y_1)

The effective point moment mobility, Y_i^e for the infinite thin plate at point i on the line moment is therefore:

$$Y_i^{e,\infty} = \frac{j\omega\theta_i^u}{M_i^u} = \frac{j\omega}{M_i^u}\int_a^b \theta_u{}'(r)dr \tag{26}$$

where M_i^u, is the excitation moment at i^{th} connection point. Extending the same method to an infinite plate attached with a PZT patch actuator and considering pure line moments are induced at the edges as depicted in Figure 6, the effective point moment mobility at point $(x_{\dot{\theta}_{x1}}, y_{\dot{\theta}_{x1}})$ can be evaluated by considering the line moments of the PZT patch separately.

Assuming the moment excitation is uniform along the line, the effective line moment mobility, Y_∞^{eff} can be obtained as summation of Y_i^e for all connection points. In this case, the connection point is assumed to be along the length of the edges of the PZT patch or can be simply put as integration along the patch length in x and y direction:

$$Y_\infty^{eff} = \int_u Y_i^e \, du = \int_u \frac{j\omega\theta_i^u}{M_i^u} du \tag{27}$$

Essentially, Y_∞^{eff} is the inverse of mechanical impedance as seen by the Non-DS by the line moments of the patch, Z_∞. Since the average mobility of a randomized thin plate can be well-approximated to be the mobility of an infinite thin plate, the solutions for Eq. (27) are obtained numerically using computational software and will be compared with its finite model for verification.

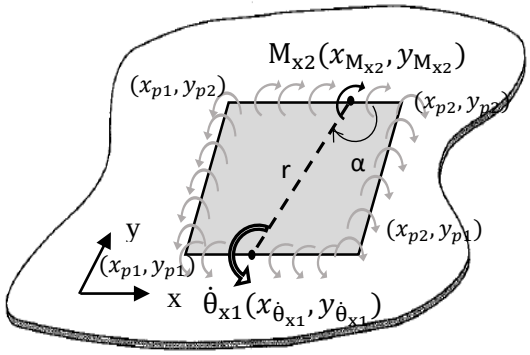

Figure 6: Induced line moments and resulting angular velocity, $\dot{\theta}_{x1}$ on the PZT patch

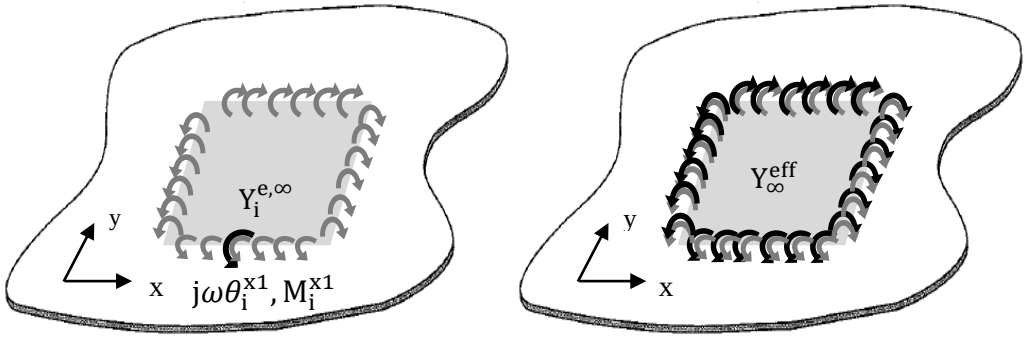

Figure 7: Illustration of effective point moment mobility at one point on line x_1 (LEFT), effective line moment mobility of the infinite thin plate (RIGHT)

3.3 Finite mobilities model

The finite model for effective line moment mobility on a randomized thin plate can be written as:

$$Y_{fin}^{eff} = \int_u Y_i^{e,fin}\, du = \int_u \frac{\dot{\theta}_u^i}{M_{pzt,u}^i} du$$
$$= \int_u [(Y_{\dot{\theta}_u^i, M_{pzt,x1}} * M_{pzt,x1} - Y_{\dot{\theta}_u^i, M_{pzt,x2}} * M_{pzt,x2})$$
$$+ (Y_{\dot{\theta}_u^i, M_{pzt,y1}} * M_{pzt,y1} - Y_{\dot{\theta}_u^i, M_{pzt,y2}} * M_{pzt,y2})] du / M_{pzt,u}^i \quad (28)$$

Assuming the moment magnitude is uniform along the line, Eq. (28) is simplified to be:

$$Y_{fin}^{eff} = \int_{x_{p1}}^{x_{p2}} (Y_{\dot{\theta}_u^i, M_{pzt,x1}} + Y_{\dot{\theta}_u^i M_{pzt,x2}}) dx + \int_{y_{p1}}^{y_{p2}} (Y_{\dot{\theta}_u^i, M_{pzt,y1}} + Y_{\dot{\theta}_u^i, M_{pzt,y2}}) dy \quad (29)$$

where,

$$Y_{\dot{\theta}_{x,y} M_{pzt,x1}} = \frac{\dot{\theta}_{x,y}}{M_{pzt,x1}} = j\omega \sum_{m=1}^{\infty} \sum_{n=1}^{\infty} \frac{\Psi_{mn}^{x,y} \vartheta_{m,n}^{x1,y}}{-\omega^2 M_{mn} + K_{C,mn}} \quad (30)$$

$$Y_{\dot{\theta}_{x,y} M_{pzt,x2}} = \frac{\dot{\theta}_{x,y}}{M_{pzt,x2}} = j\omega \sum_{m=1}^{\infty} \sum_{n=1}^{\infty} \frac{\Psi_{mn}^{x,y} \vartheta_{m,n}^{x2,y}}{-\omega^2 M_{mn} + K_{C,mn}} \quad (31)$$

$$Y_{\dot{\theta}_{x,y} M_{pzt,y1}} = \frac{\dot{\theta}_{x,y}}{M_{pzt,y1}} = j\omega \sum_{m=1}^{\infty} \sum_{n=1}^{\infty} \frac{\Psi_{mn}^{x,y} \vartheta_{m,n}^{x,y1}}{-\omega^2 M_{mn} + K_{C,mn}} \quad (32)$$

$$Y_{\dot{\theta}_{x,y} M_{pzt,y1}} = \frac{\dot{\theta}_{x,y}}{M_{pzt,y2}} = j\omega \sum_{m=1}^{\infty} \sum_{n=1}^{\infty} \frac{\Psi_{mn}^{x,y} \vartheta_{m,n}^{x,y2}}{-\omega^2 M_{mn} + K_{C,mn}} \quad (33)$$

The term $\Psi_{mn}^{x,y}$ is the first derivative of ϕ_{mn} with reference to *x* and *y* respectively i.e. the shape function for angular displacement:

$$\Psi_{mn}^{x,y} = -sin(\beta_p) \frac{\partial \phi_{mn}(x,y)}{\partial x} + cos(\beta_p) \frac{\partial \phi_{mn}(x,y)}{\partial y} \quad (34)$$

β_p is the orientation angle of the angular displacement on the plate. The terms $\vartheta_{m,n}^{x1,y}$, $\vartheta_{m,n}^{x2,y}$, $\vartheta_{m,n}^{x,y1}$ and $\vartheta_{m,n}^{x,y2}$ are the shape functions for line moments at each of the edge of the patch which can be combined by taking $\vartheta_{m,n}^{x,y}$ as the total shape function of the line moment at each of the PZT edges thru the following relationship:

$$\vartheta_{mn}^{x,y} = (\vartheta_{m,n}^{x1,y} - \vartheta_{m,n}^{x2,y}) + (\vartheta_{m,n}^{x,y1} - \vartheta_{m,n}^{x,y2})$$
$$= \left[\frac{n}{m}\frac{L_x}{L_y} + \frac{m}{n}\frac{L_y}{L_x}\right] * \left[cos\left(\frac{m\pi x_{c1}}{L_x}\right) - cos\left(\frac{m\pi x_{c2}}{L_x}\right)\right]\left[cos\left(\frac{n\pi y_{c1}}{L_y}\right) - cos\left(\frac{n\pi y_{c2}}{L_y}\right)\right] \quad (35)$$

where x_{c1}, x_{c2}, y_{c1} and y_{c2} are the coordinates of the corner of the patch on the thin plate. The conversion terms mentioned in Eq. (21) can now be defined. The term $\varphi_{M_{line}}$ is essentially Eq.

(34) and the shape function for angular velocity along the edges of the patch for line connection, $\varphi_{\dot{\theta}_{line}}$ is:

$$\varphi_{\dot{\theta}_{line,k}} = \varphi_{\dot{\theta}_{x1,along\ py1}} + \varphi_{\dot{\theta}_{x2,along\ py2}} + \varphi_{\dot{\theta}_{y1,along\ px1}} + \varphi_{\dot{\theta}_{y2,along\ px2}} \quad (36)$$

$$= \int_{px1}^{px2} (\Psi_{mn}^{x,y=py1} + \Psi_{mn}^{x,y=py2})dx + \int_{py1}^{py2} (\Psi_{mn}^{x=px1,y} + \Psi_{mn}^{x=px2,y})dy \quad (37)$$

The theoretical shunt impedance $Z_{sh,k}$ in Eq. (22) can be solved accordingly.

3.2 Simulation results

Figure 8 showed the comparison between ensemble average of finite model and the estimation of effective line moment mobility, Y_{∞}^{eff}. The estimation curves (dashed black) showed good agreement with the average responses for each case. It is important to note that the randomized finite plate still exhibit distinct modes at frequency range where MOF<2, therefore the response is still strongly-dependent on the location of measurement and boundary conditions of the structure. At MOF>2 range, broader peaks can be seen, signifying high modal overlapping of the response. At this range, the response is highly sensitive to uncertainties, however boundary condition will have no effect and the average response will appear the same regardless of where measurement is taken [4] [21]. A smoother average response for the randomized plate can be achieved at this range by taking higher number of ensemble for Monte Carlo simulation.

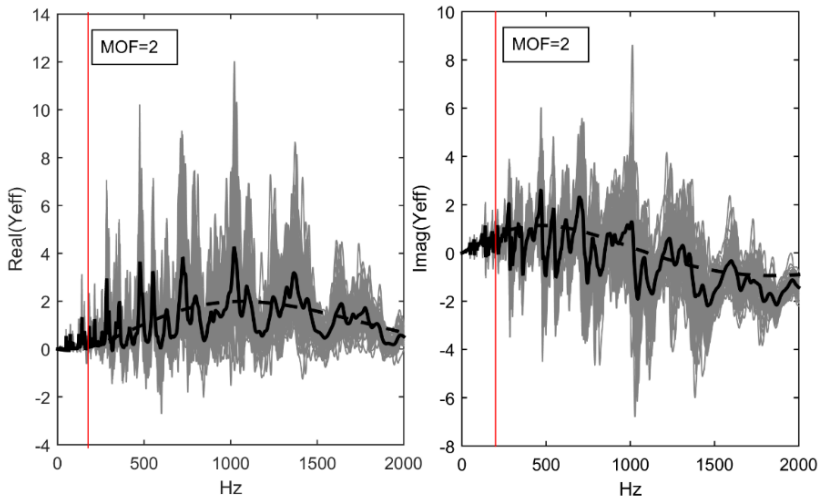

Figure 8: Real values (left) and imaginary values (right) of effective line moment mobility of the randomized thin plate (grey, 50 ensembles) and its average (solid black) Eq. (29), and the effective line moment mobility for infinite thin plate as in Eq. (27) (dashed black)

From this study, it is shown that the effective line moment mobility of a non-deterministic thin plate can be estimated using double integration of the infinite point moment mobility; i.e. integrating point moment mobility to get effective point moment mobility, and integrating the effective point moment mobility to get effective line moment mobility. It is also essential to

mention that the analytical model managed to significantly cut computational time to ~40 times shorter compared to using the finite method via Monte Carlo simulation which requires high number of degrees of freedom for modal summation, and large number of ensembles in order to completely model the response for high frequency range.

4.0 IMPLEMENTATION OF ELECTRICAL SHUNT CIRCUIT FOR MAXIMUM ENERGY DISSIPATION FROM A NON-DS

4.1 Introduction

This section will discuss the methods used to design and implement the electrical shunt circuit, Z_{sh} for maximum power dissipation from a non-deterministic thin plate as derived previously. The goal here is to design a realizable PZT shunt damper circuit using the *RLC* analog circuitry components and to show the energy harvesting from fhe non-deterministic thin plate accordingly. A benchmark model consists of a randomized thin plate attached with six evenly distributed PZT shunt dampers with their optimal shunt circuits is taken for this study. The equivalent circuit is designed using MULTISIM 12.0 software and integrated into COMSOL 4.4 using SPICE netlist for validation thru virtual experiment.

4.2 Possible circuit design

Intuitively, the number of possible *RLC* circuit configurations that can resemble both real and imaginary parts of impedance $Z_{sh,k}$ is infinite. For this study, only one is needed for implementation purpose. Through heuristic method, one of the simplest circuit configuration found is in the following form:

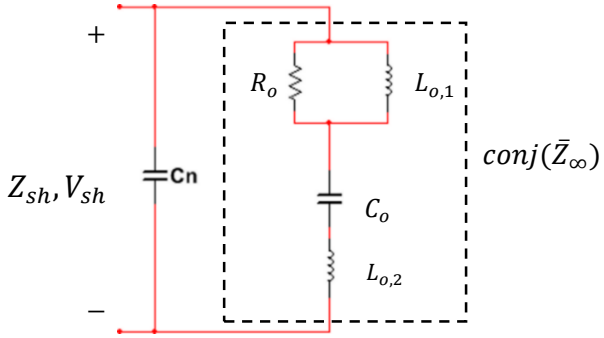

Figure 9: One of possible configuration for equivalent circuit to recreate impedance in Eq. (22)

$$Z_{sh,k} = \frac{1}{j\omega C_n} || \left(\frac{j\omega R_o L_{o,1}}{j\omega L_{o,1} + R_o} + \frac{1}{j\omega C_o} + j\omega L_{o,2} \right) \tag{38}$$

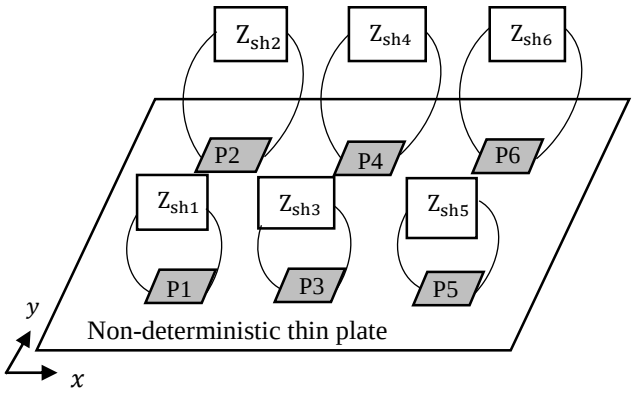

Figure 10: Illustration of six equally-distributed PZT patches with individual electrical shunt circuits on a non-deterministic thin plate

The circuit configuration in Figure 9 is acquired by keeping in mind that expression $conj(\bar{Z}_{\infty,j}||Z_{Cp,j})$ from Eq. (22) is also equivalent to $conj(\bar{Z}_{\infty,j})||conj(Z_{Cp,j})$. Hence, the capacitor C_n is designed individually in one branch to specifically cancel out the inherent capacitance of the PZT patch by making it as the complex conjugate of C_p. By doing this, only the value of C_n needs to be modified when different PZT patch is used without having to change the values of the other circuit components R_o, $L_{o,1}$, C_o and $L_{o,2}$, to recreate $conj(\bar{Z}_{\infty})$. The value of C_n needs to be negative for it to be complex conjugate of C_p, therefore negative capacitance method will be employed. According to work by Moheimani and his co-workers, a negative capacitance 2-5% greater than the PZT capacitance will provide good damping performance with acceptable robustness to small changes in environmental temperature, and also to ensure stability [8]. Therefore, the impedance of C_n is taken to be 2% larger than the PZT capacitance i.e. $Z_{cn} = -1/(j\omega * 1.02 * C_p)$.

The focus now is to design the circuit branch for $conj(\bar{Z}_{\infty,k})$. By utilizing the MATLAB function `lsqnonlin` for optimization routine, the values for R_o, $L_{o,1}$, C_o and $L_{o,2}$ arranged in circuit shown in Figure 9 can be determined in order to get the best curve that resembles $conj(\bar{Z}_{\infty})$. Since the interest of this research is at frequencies where MOF>2, the curve optimization is performed starting from frequency 190Hz and above. Table 1 shows the values for circuit components for all six PZT shunt dampers resulting from the optimization, assuming identical patches are used.

Table 1: Values of electronic components for shunt circuit in Figure 10

	P1	**P2**	**P3**	**P4**	**P5**	**P6**
R_o (kΩ)	2.755	4.512	2.795	4.584	2.755	4.419
$L_{o,1}$ (H)	3.215	4.784	3.122	4.490	3.225	4.902
C_o (nF)	-98.02	-61.11	-97.39	-60.69	-97.96	-60.69
$L_{o,2}$ (H)	-0.1645	-0.2695	-0.1669	-0.2752	-0.1645	-0.2645
C_n (nF)	-92.68					

Figure 11 illustrates the total circuit impedance built using the components tabulated in Table 1 versus the theoretical impedance shown in Eq. (22).

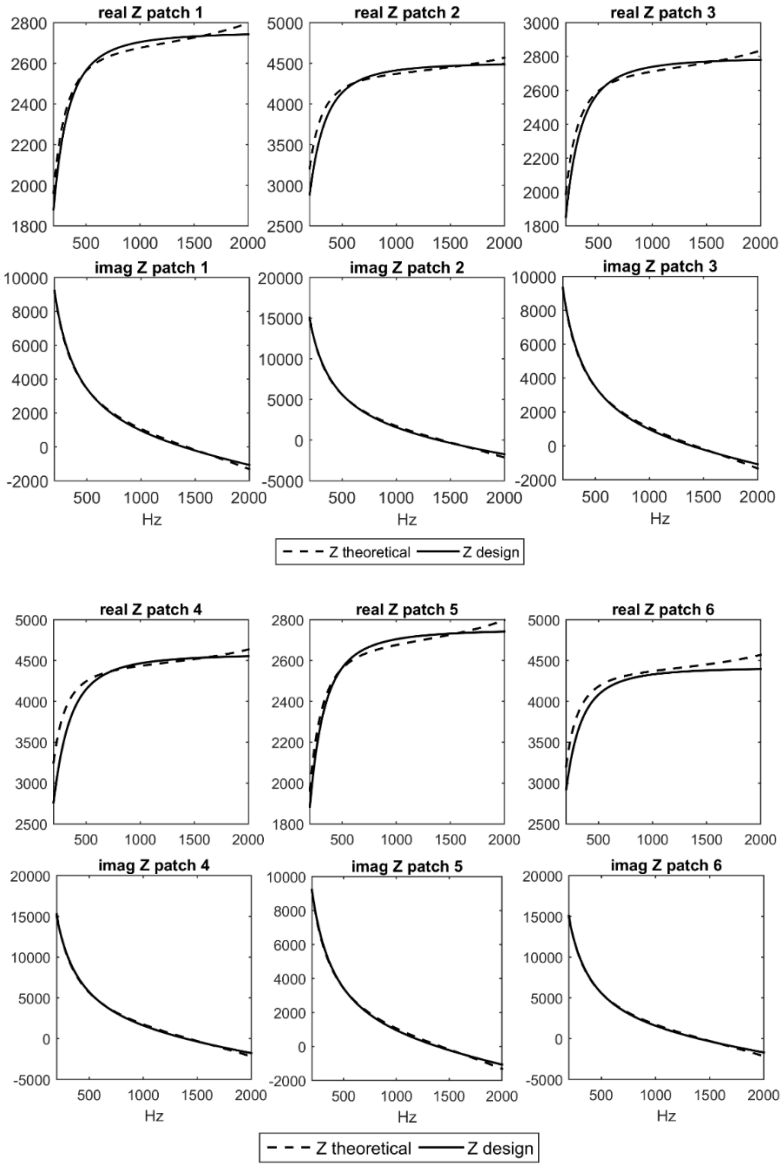

Figure 11: Comparison of real and imaginary values of shunt circuit impedance; theoretical using Eq. (22) (dashed), designed using configuration in Figure 9 and component values from Table 1 (solid)

From Table 1, negative values for capacitor C_o and inductor $L_{o,2}$ are needed and since passive electronic components cannot realize negative values, the concept of negative impedance converter will be employed. Negative impedance converter is a one-port non-inverting op-amp circuit using at least three electronic components to produce a negative impedance Z_{in} as seen by the source:

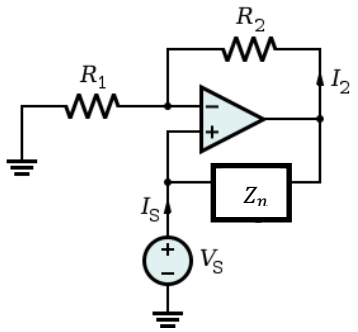

Figure 12: A negative impedance converter employing non-inverting op-amp

The op-amp output voltage is:

$$V_{op} = V_S\left(1 + \frac{R_2}{R_1}\right) \tag{39}$$

The current going from the op-amp output through component with impedance Z_n toward the source V_S is $-I_S$:

$$-I_S = \frac{V_{op} - V_S}{Z_n} = V_S \frac{\frac{R_2}{R_1}}{Z_n} \tag{40}$$

Therefore, the NIC serves its purpose where the impedance as seen by the source can be written as:

$$Z_{in} = \frac{V_S}{-I_S} = -Z_n \frac{R_1}{R_2} \tag{41}$$

The negative impedance $Z_n$can be resistors, capacitors, inductors or any impedance network of interest. Here, R_1 and R_2 act as the multiplier to $-Z_n$ so that the impedance value can be adjusted accordingly. Implementing *NIC*, the circuit configuration in Figure 9 can be further refined to be in the form of op-amp networks as follows:

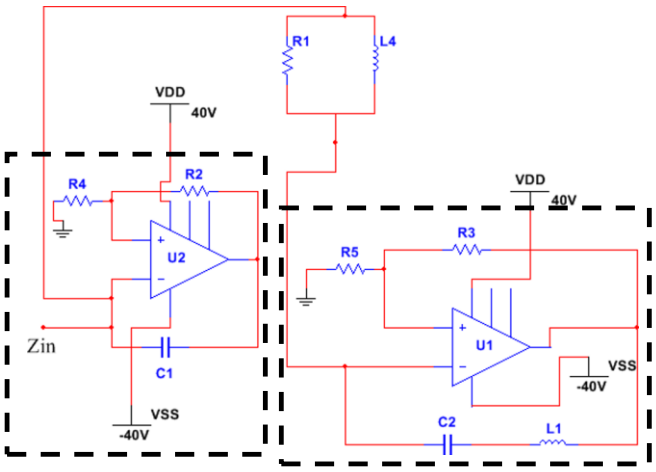

Figure 13: Refined circuit from Figure 9 employing NIC using op-amp network

The term Z_{in} in Figure 13 is the total impedance of the circuit network which is the same as shunt impedance, Z_{sh}. Op-amp networks labelled as *U1* and *U2* in the figure are *NIC*s producing the following impedances:

$$Z_{U1} = -(\frac{1}{j\omega C2} + j\omega L1) \tag{42}$$

$$Z_{U2} = -\frac{1}{j\omega C1} \tag{43}$$

For implementation of electrical circuit in COMSOL 4.4, the op-amps in *NIC* networks in Figure 13 needs to be redefined into more primitive circuitry components. Figure 14 shows the schematic of the total shunt circuit impedance for the first patch, P1 only, by using the SUBCIRCUIT definition to replicate the op-amp. Since the circuit for each PZT shunt dampers on the thin plate are independently connected, the other circuits: Z_{sh2}, Z_{sh3}, Z_{sh4}, Z_{sh5}, and Z_{sh6} are created in similar manner by using the circuit components for respective patch, as tabulated in Table 1. The shunt circuit for the six PZT shunt dampers can now be implemented into COMSOL 4.4 in terms of SPICE netlists for demonstration of Non-DS energy suppression.

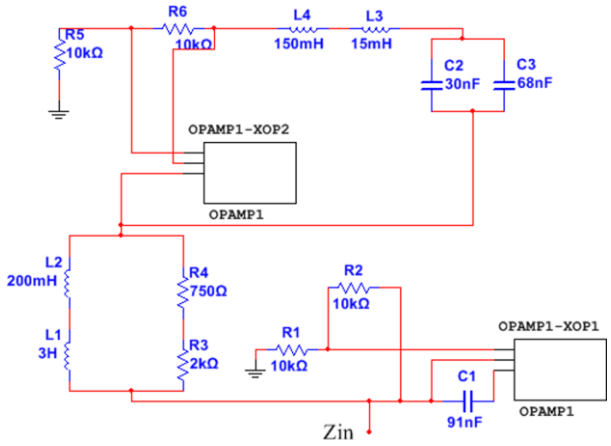

Figure 14: MULTISIM schematic for shunt circuit network for patch 1, Z_{sh1} using Op-amp subcircuit

Figure 15 shows the ratio between open-circuit energy and closed-circuit (with optimal shunt circuit) energy of the plate model in COMSOL 4.4. The open-circuit and closed-circuit conditions of the plate is achieved by letting current, *Q=0* and connecting the terminal of the circuit to the SPICE netlist, respectively. From the simulation result, good agreement between the theoretical energy curve derived in Eq. (6) with the ensemble average response can be seen especially at range MOF>2.

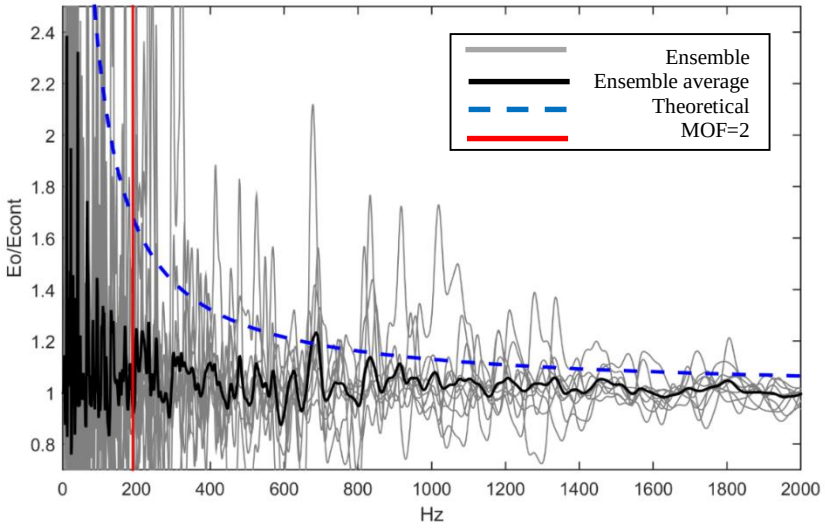

Figure 15: Energy ratio E_0/E_{cont} obtained via virtual experiment using COMSOL for 20 ensembles

Therefore, the energy reduction (harvesting) ratio curve (Eq. (6)) can be treated as the maximum energy harvesting achievable of a Non-DS when directly connected with optimal controllers.

Conclusions

For conclusions, it is found out that in order to maximize energy dissipation from a Non-DS using a PZT shunt damper, the shunt circuit impedance needs to be the complex conjugate of its inherent capacitance parallel with electrical-equivalent impedance of its non-deterministic host structure at their respective line connection. The impedance is found using the inverse of effective line moment mobility of an infinite thin plate, Y_{∞}^{eff} acquired using double integration of the driving point moment mobility of an infinite thin plate. The theoretical estimation managed to significantly cut computational time and resource to model mobility of a Non-DS. This work also showed one realizable shunt circuit to imitate the theoretical impedance using *RLC* components which later implemented into COMSOL using SPICE netlist to for virtual experiment. The results showed good agreement between the ensemble averages with theoretical curve which serves as an envelope for the highest energy dissipation attainable from a Non-DS when directly attached with optimal controllers. Analysis also showed that by using more PZT shunt dampers, better energy harvesting can be achieved however more weight and stiffness is added to the structure which is not usually favorable. Therefore, the number of optimal PZT shunt damper used (or generally, number of controllers used) and the desired control effect on the Non-DS needs to be compensated.

Acknowledgement

This work was supported by Fundamental Research Grant Scheme (FRGS15-165-0406) from the Ministry of Higher Education Malaysia.

References

[1] F. J. Fahy, "Statistical energy analysis: a critical overview," *Philosophical Transactions of the Royal Society of London. Series A: Physical and Engineering Sciences,* vol. 346, pp. 431-447, 1994.

[2] F. J. Fahy and P. Gardonio, *Sound and structural vibration: radiation, transmission and response*: Academic press, 2007.

[3] R. S. Langley and A. N. Bercin, "Wave intensity analysis of high frequency vibrations," *Philosophical Transactions of the Royal Society of London. Series A: Physical and Engineering Sciences,* vol. 346, pp. 489-499, 1994.

[4] C. Manohar and A. Keane, "Statistics of energy flows in spring-coupled one-dimensional subsystems," *Philosophical Transactions of the Royal Society of London. Series A: Physical and Engineering Sciences,* vol. 346, pp. 525-542, 1994.

[5] R. S. Langley, "Mid and high-frequency vibration analysis of structures with uncertain properties," in *11th International Congress on Sound and Vibration* St. Petersburg, Russia, 2004.

[6] A. G. Muthalif and R. S. Langley, "Active control of high-frequency vibration: Optimisation using the hybrid modelling method," *Journal of Sound and Vibration,* vol. 331, pp. 2969-2983, 2012.

[7] R. Langley and P. Bremner, "A hybrid method for the vibration analysis of complex structural-acoustic systems," *The Journal of the Acoustical Society of America,* vol. 105, p. 1657, 1999.

[8] S. R. Moheimani and A. J. Fleming, *Piezoelectric transducers for vibration control and damping*: Springer, 2006.

[9] S. Behrens, A. Fleming, and S. Moheimani, "A broadband controller for shunt piezoelectric damping of structural vibration," *Smart Materials and Structures,* vol. 12, p. 18, 2003.

[10] P. J. Shorter and R. S. Langley, "On the reciprocity relationship between direct field radiation and diffuse reverberant loading," *The Journal of the Acoustical Society of America,* vol. 117, pp. 85-95, 2005.

[11] J. Liang and W.-H. Liao, "Impedance modeling and analysis for piezoelectric energy harvesting systems," *IEEE/ASME Transactions on Mechatronics,* vol. 17, pp. 1145-1157, 2012.

[12] A. Cicirello and R. S. Langley, "Efficient parametric uncertainty analysis within the hybrid Finite Element/Statistical Energy Analysis method," *Journal of Sound and Vibration,* vol. 333, pp. 1698-1717, 2014.

[13] L. Benassi and S. Elliott, "The equivalent impedance of power-minimising vibration controllers on plates," *Journal of Sound and Vibration,* vol. 283, pp. 47-67, 2005.

[14] N. W. Hagood and A. von Flotow, "Damping of structural vibrations with piezoelectric materials and passive electrical networks," *Journal of Sound and Vibration,* vol. 146, pp. 243-268, 1991.

[15] C. Norwood, H. Williamson, and J. Zhao, "Surface mobility of a circular contact area on an infinite plate," *Journal of Sound and vibration,* vol. 202, pp. 95-108, 1997.

[16] L. Cremer, M. Heckl, and B. A. Petersson, *Structure-borne sound: structural vibrations and sound radiation at audio frequencies*: Springer, 2005.

[17] P. Hammer and B. Petersson, "Strip excitation, part I: strip mobility," *Journal of Sound and Vibration,* vol. 129, pp. 119-132, 1989.

[18] Y. Li and J. Lai, "Prediction of surface mobility of a finite plate with uniform force excitation by structural intensity," *Applied Acoustics,* vol. 60, pp. 371-383, 2000.

[19] J. Dai, J. Lai, Y. Li, and H. Williamson, "Surface mobility over a square contact area of an infinite plate: experimental measurements and numerical prediction," *Applied Acoustics,* vol. 60, pp. 81-93, 2000.

[20] S. Ljunggren, "Line mobilities of infinite plates," *The Journal of the Acoustical Society of America,* vol. 86, pp. 1419-1431, 1989.

[21] R. H. Lyon, *Statistical energy analysis of dynamical systems: theory and applications*: MIT press Cambridge, MA, 1975.